

AN APPROACH TO EFFECTIVE TEMPERATURE AND SURFACE GRAVITY IN POST-AGB AND RV TAURI STARS AT THE NEAR-IR REGION

R. E. Molina,¹

Received November 19, 2018; accepted November 19, 2018

RESUMEN

Se determina la temperatura efectiva y la gravedad superficial de un conjunto de estrellas evolucionadas post-AGB y RV Tau a partir de ecuaciones empíricas usando como calibradores los colores intrínsecos de la fotometría 2MASS (Two Micron All Sky Survey). Analizamos un total de 36 estrellas donde 25 de ellas son post-AGB y las restantes 11 son RV Tau respectivamente. Utilizamos un grupo de 11 estrellas con medidas de paralaje como calibradores en la determinación de la magnitud absoluta en la banda J. Los resultados para la T_{eff} y la $\log g$ derivadas de los colores intrínsecos $(J-H)_0$ y $(H-K_s)_0$ alcanzan una dispersión de 220 K y 0.27, respectivamente. Estimamos la magnitud absoluta en la banda J con una precisión de 0.28 mag, esto nos indica que los colores $(J-H)_0$ y $(H-K_s)_0$ presentan sensibilidad a dicho parámetro.

ABSTRACT

A number of empirical correlations that allows us to calculate the effective temperature and surface gravity for a set evolved post-AGB and RV Tauri stars are determined using as calibrators the intrinsic colours of 2MASS (Two Micron All Sky Survey) photometry. We have analyzed a total sample of 36 stars where 25 are post-AGB stars and 11 are RV Tauri stars, respectively. A group of 11 stars with parallaxes measures were used as calibrators of the absolute magnitude. The result for T_{eff} and $\log g$ from intrinsic colours $(J-H)_0$ and $(H-K_s)_0$ at the near-infrared pass bands reach a dispersion of 220 K and 0.27, respectively. We can estimate the absolute magnitude using the intrinsic colour in the near-infrared band with an uncertainty of 0.28 mag. This indicates that $(J-H)_0$ and $(H-K_s)_0$ show sensitivity to the absolute magnitude.

Key Words: FUNDAMENTAL PARAMETERS: T_{EFF} , $\text{LOG } G$ AND M_V ; STARS: POST-AGB–RV TAURI STARS.

1. INTRODUCTION

Post-AGB stars are low and intermediate mass stars ($0.8 - 8 M_{\odot}$) that have passed the asymptotic giant branch (AGB) and are on their way toward the planetary nebula (PN) phase. On the other hand, RV Tauri stars are very luminous and variable stars ($M_V \approx -3$ mag) with spectral types F, G and K which have an infrared excess attributed to the mass lost in the AGB phase (Preston 1963; Jura 1986; Wahlgren 1993). According to RV Tauri stars' infrared and statistical properties, Jura (1986) suggests that the RV Tauri stars are also post-AGB

stars. The determination of fundamental physical parameters for these types of objects (post-AGB and RV Tauri) such as effective temperature and surface gravity are obtained from the ionization balance for elements with two states of ionization (e.g. the ratio of iron Fe I/Fe II) using atmospheric models for this purpose (see Giridhar et al. 2010 paper I).

Alternatively, attempts have been made to derive a set of functional relationships that allow to estimate these parameters from correlations with photometric data for these objects. The proposed first attempts were carried out by Arellano Ferro et al. (1990), Arellano Ferro y Mantegazza (1996) using the reddening-free indexes $[c_1]$, $[m_1]$ and $[u-v]$ from Strömgren photometry. Later, Arellano Ferro (per-

¹Laboratorio de Investigación en Física Aplicada y Computacional, Universidad Nacional Experimental del Táchira, Venezuela.

sonal communication) found functional relationships involving the effective temperature and photometric indexes $[c_1]$, $[m_1]$ and $[u-v]$ using 41 bright supergiant stars with classes I and II with spectral types within the range of A0–K0 from Bravo-Alfaro et al. (1997). However, these relations were never published since their intrinsic dispersion was large, probably due to the limited quality of used temperature data.

Recently, Arellano Ferro (2010) has estimated functional relationships from a set of 50 supergiant stars with spectral types F–G including some objects like stars evolved post-AGB and RV Tauri stars (see Stasińska et al. 2006). For calibration, A. Ferro uses data from a homogeneous sample of temperature and gravity taken from Lyubimkov et al. (2010). This author concludes that the temperature can be obtained with good accuracy from the reddening-free indexes $[c_1]$ and $[m_1]$ (e.g. ± 152 K for both indexes) while gravity can be calculated from index $\Delta[c_1]$ with an uncertainty of 0.26 dex. However, although there is a correlation between the absolute magnitude M_V and the index $\Delta[c_1]$, this correlation is less satisfactory.

In the near-infrared region, 2MASS catalogue (Cutri et al. 2003) provides the most complete database of near infrared Galactic point sources available to date. Various jobs in this region have shown the dependence of atmospheric parameters with the de-reddened colours (Bessell & Brett 1988; Covey et al. 2007; Bilir et al. 2008a; 2008b; 2009; Straizys & Lazauskaite 2009; Yaz et al. 2010). Bilir et al. (2008a) obtained the transformation formulae between JHK_s photometry system to BVRI and SDSS gri photometric systems for the main sequence stars. These transformations provide absolute magnitude and distance determinations which can be used in space density evaluations at short distances were some or all of the gri magnitudes are saturated. These authors also showed that those formulae were sensitive to metallicity. In other similar studies (Bilir et al. 2008b; Bilir et al. 2009) the calculated absolute magnitudes were compared with Pickles (1998)’ synthetic data and the results were in good agreement with synthetic library results. In recent study (Yaz et al. 2010) it was obtained the transformation formulae for the conversion between JHK_s photometry system to BVRI, and SDSS gri photometric systems for set of giant stars. These formulae are directly dependent on metallicity as well and also provide absolute magnitude and distance determinations for this type of population.

In this paper we introduce for the first time two functional relationships that allow us to estimate the

effective temperature and gravity in post-AGB and RV Tauri stars from their infrared colours. These equations are valid for evolved stars of low and intermediate masses ($1 < M_{\odot} \leq 4$) in which the central star is visible due to the low opacity of the dust that surround them. However, most of these objects radiate in the infrared range and are, therefore, detectables by 2MASS source. Furthermore, these equations can not be applied to massive post-AGB objects, i.e., $4 < M_{\odot} \leq 8$, without optical counterpart owing to a dense circumstellar material that obscures the central star. More massive objects will have more material in their circumstellar shells and the star will be quite obscured, while it will not be in the case of objects will less material in the envelope. Sources with dusty shells will therefore be fainter at optical wavelengths but brighter in the infrared. Inhomogeneous sample from several authors and the compilation of Stasińska et al. (2006) have been used as calibrators. We attempt to recover the absolute magnitude from the intrinsic colour despite the lack of homogeneity and the limitations on the parallax of the sample.

The structure of the paper is as follows: Sect. 2 introduces the data used and the criteria applied to estimate the colour excess. Sect. 3 shows the functional relationships for atmospheric parameters using intrinsic colours. Sect. 4 deals with a relationship to estimate the absolute magnitude in the J passband using as calibrators the available Hipparcos trigonometric parallax measurements. Finally, in Sect. 5 we discuss our results.

2. DATA

For post-AGB stars the temperature and gravity used in our calibration come mainly from the compilation made by Stasińska et al. (2006) while for RV Tauri stars are obtained from Giridhar et al. (2005). We select the atmospheric parameters for a set of 24 post-AGB stars and 11 RV Tauri stars, respectively (see column 8 of table 1). A group of 11 stars with Hipparcos parallax measurements were used as calibrators of the absolute magnitude (see Table 3). Most stars were selected with intermediate and high galactic latitude to reduce the contribution of the observed extinction. Stars identified on the galactic plane were chosen to have parallax measurements. Figure 1 shows the unreddened colour-colour diagram of the post-AGB (filled triangles) and RV Tauri (open squares) stars. We notice that there is a good correlation between the sample with a large dispersion probably due to the dependence on metallicity. Some objects in the sample show a greatest colour

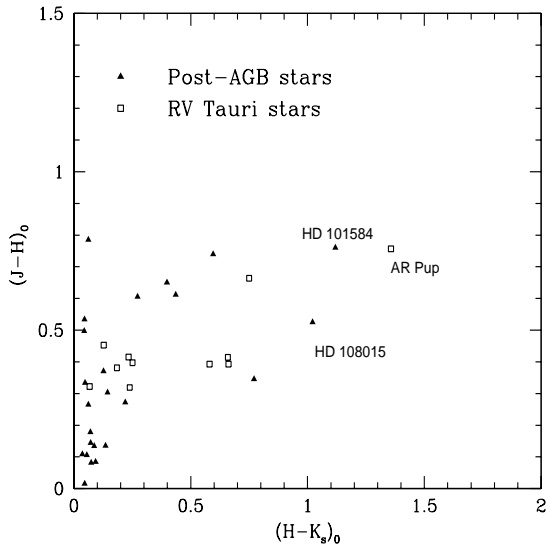


Fig. 1. The $J-H$ vs. $H-K_s$ diagram for unreddened all stars of the sample. The filled triangles represent the post-AGB stars and open squares to the RV Tauri stars.

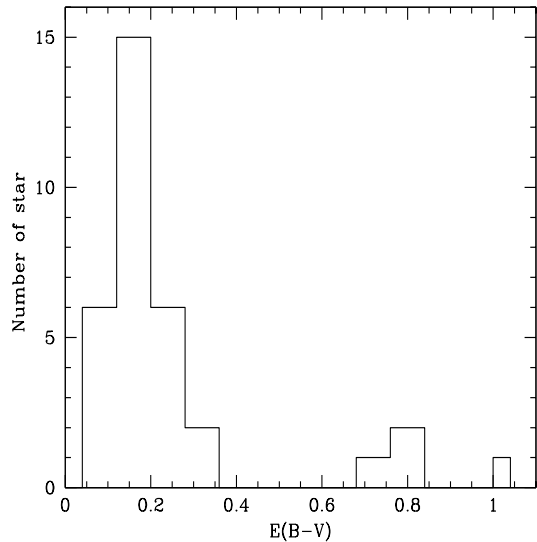


Fig. 2. The distribution of the total $E(B-V)$ found for our sample.

$(H-K_s) > 1.0$, e.g. AR Pup, HD 101584 and HD 108015. This excess seen in the $(H-K_s)$ colour may be due to the contribution of the circumstellar component since the contribution of interstellar dust has been removed (for details see Section 3).

We studied the post-AGB and RV Tauri stars with A–G spectral type within the range in effective temperature and gravity between 5000–8500 K and 0.0–2.0, respectively. According to SIMBAD² source a few post-AGB stars in the sample are considered semi-regular pulsating stars, while the RV Tauri are mostly variable stars with exception of HP Lyr (eclipsing binary star) and UY CMa (semi-regular pulsating star). These objects are indicated by the upper subscripts "a", "b" and "c". Table 1 contains the fundamental atmospheric parameters for the total number of stars studied. Columns are organized according to the type of star and the HD number as follows: name of stars, spectral type, galactic coordinates, effective temperature, surface gravity, comment and references.

The trigonometric parallaxes used in our 11 stars were taken from the current reduced Hipparcos catalogue (van Leeuwen 2007). The JHK_s photometry was taken from 2MASS (Cutri et al. 2003) source.

3. REDDENING ESTIMATION

Light coming from a star is attenuated and reddened by material in the line of sight. Note that the total line of sight extinction is likely to contain both a circumstellar and an interstellar component. In order to perform our calibrations we need to deredden the colour indexes in the near-infrared pass-band. Unfortunately, there is no precise measurements in the literature about the colour excess for each object. To estimate the colour excess $E(B-V)$ we use the NASA Extragalactic Database (NED, based on the work of Schlegel et al. 1998).³

This model provides $E(B-V)$ from the galactic coordinates with an accuracy of 10% for stars with galactic latitudes $b > 5^\circ$. For lower latitudes their reddenings are more uncertain. The reddening estimated from NED refers to the full line of sight and should be applied as it stands only to extragalactic objects or objects well about the dust layer. Several studies have noticed that the dust model of Schlegel et al. (1998) overpredict $E(B-V)$ when $E(B-V)_{NED} > 0.15$ (see e.g., Arce & Goodman 1999; Beers et al. 2002; Yasuda et al. 2007). In this sense we adopt the correction as suggested by Bonifacio, Monai & Beers (2000a)⁴. On the other hand for those stars in the dust layer the colour excess along the line of sight must be estimated assuming that the dust in the Galactic disk can be modelled as a thin expo-

²<http://simbad.u-strasbg.fr/simbad/>

³<http://nedwww.ipac.caltech.edu/forms/calculator.html>

⁴ $E(B-V) = 0.10 + 0.65 [E(B-V)_{NED} - 0.1]$

TABLE 1

THE FUNDAMENTAL ATMOSPHERIC PARAMETERS FOR THE SAMPLE POST-AGB AND RV TAURI USED AS CALIBRATORS. THE SOURCES OF TEMPERATURE AND GRAVITY ARE RESPECTIVELY BY THE NUMBERS IN COLUMN 8.

Star	SpT.	l ($^{\circ}$)	b ($^{\circ}$)	T_{eff} (K)	$\log g$	comment	Refs.
HD 27381	F2	161.63	-08.07	7500±250	1.0±0.5	post-AGB	(01)
HD 46703	F7IVw	161.98	+19.59	6000±150	0.4±0.3	post-AGB ^a	(02)
HD 56126	F5Iab	206.74	+09.99	7250±200	0.5±0.5	post-AGB ^a	(16)
HD 95767	F3II	290.53	-01.95	7300±300	1.5±0.25	post-AGB	(11)
HD 101584	F0Iap	293.02	+05.93	8500±500	1.5±0.5	post-AGB	(03)
HD 107369	A2II/III	295.47	+29.86	7600±200	1.5±0.25	post-AGB	(11)
HD 108015	F4Ib/II	298.25	+15.47	6800±200	1.25±0.25	post-AGB ^a	(11)
HD 112374	F3Ia	304.34	+36.39	6000±275	0.6±0.3	post-AGB ^a	(12)
HD 114855	F5Ia/Iab	306.24	+08.03	6000±200	0.5±0.25	post-AGB	(10)
HD 116745	F0Ibp	309.07	+15.17	6950±75	1.15±0.1	post-AGB	(13)
HD 133656	A1/A2Ib/II	325.03	+08.64	8000±200	1.25±0.25	post-AGB	(14)
HD 148743	A7Ib	007.95	+26.70	7200±500	0.5±0.3	post-AGB	(04)
HD 161796	F3Ib	077.13	+30.86	6666±500	0.7±0.3	post-AGB ^a	(08)
HD 163506	F2Ib	051.53	+23.28	6550±500	0.6±0.3	post-AGB ^a	(02)
HD 172481	F2Ia	006.72	-10.73	7250±200	1.5±0.25	post-AGB ^a	(15)
HD 179821	G5Ia	035.61	-04.95	6800±150	1.3±0.5	post-AGB ^a	(05)
HD 190390	F1III	030.59	-21.53	6600±500	1.6±0.64	post-AGB ^a	(04)
CpD-625428	A7Iab	326.20	-11.11	7250±200	0.5±0.25	post-AGB	(10)
IRAS05113+1347	G8Ia	188.85	-14.29	5250±150	0.25±0.5	post-AGB	(17)
IRAS05341+0852	F4Iab:	196.18	-12.14	6500±250	1.0±0.5	post-AGB	(18)
IRAS07430+1115	G5Ia	208.93	+17.06	6000±250	1.0±0.25	post-AGB	(21)
IRAS18095+2704	F3Ib	053.83	+20.18	6500±150	0.5±0.5	post-AGB	(20)
IRAS19386+0155	F	040.50	-10.08	6800±100	1.4±0.2	post-AGB	(19)
IRAS22223+4327	F9Ia	096.75	-11.55	6500±350	1.0±0.3	post-AGB ^a	(22)
HD 82084	A4Ib/II	282.42	-09.23	6700±200	2.0±0.2	RV Tauri ^c	(23)
HD 105578	F7/F8Ib	295.24	+16.81	6000±250	1.0±0.5	RV Tauri ^c	(06)
HD 107439	G4Vp	297.87	+13.36	6250±250	1.25±0.5	RV Tauri ^c	(06)
HD 170756	K0III	028.49	-03.77	5900±150	1.13±0.15	RV Tauri ^c	(07)
AR Pup	F0Iab	253.02	-02.99	6300±200	1.5±0.2	RV Tauri ^c	(09)
AR Sgr	G4	012.39	-12.28	5300±200	0.5±0.2	RV Tauri ^c	(24)
HP Lyr	A6	072.01	+11.71	6300±200	1.0±0.2	RV Tauri ^b	(24)
RX Cap	G2	030.35	-24.27	5800±200	1.0±0.2	RV Tauri ^c	(24)
TX Oph	G0	024.74	+26.11	5000±200	0.5±0.2	RV Tauri ^c	(24)
UY CMa	G0V	224.75	-14.85	5500±200	0.0±0.2	RV Tauri ^a	(24)
UZ Oph	G2	028.87	+23.01	5000±200	0.5±0.2	RV Tauri ^c	(24)

^a Semi-regular pulsating stars.

^b Eclipsing binary star.

^c Variable stars of RV Tau type.

(01) Giridhar & Arellano Ferro (2005), (02) Luck & Bond (1984), (03) Sivarani et al. (1999), (04) Luck et al. (1990), (05) Začs et al. (1996), (06) Mass et al. (2002), (07) Giridhar et al. (1998), (08) Cenarro et al. (2007), (09) González et al. (1997a), (10) Giridhar et al. (2010), (11) van Winckel et al. (1997), (12) Luck et al. (1983), (13) González & Wallerstein (1992), (14) van Winckel et al. (1996), (15) Arellano Ferro et al. (2001), (16) Hrivnak & Reddy (2003), (17) Reddy et al. (2002), (18) van Winckel & Reyniers (2000), (19) Pereira et al. (2004), (20) Sahin et al. (2010), (21) Reddy et al. (1999), (22) Decin et al. (1998), (23) Giridhar et al. (1994), (24) Giridhar et al. (2005)

TABLE 2
THE TOTAL COLOUR EXCESS AND THE COLOUR EXCESS OF CIRCUMSTELLAR AND INTERSTELLAR COMPONENTS FOR COMMON OBJECTS IN BOTH SAMPLES.

IRAS/HD number	E(B-V) (observed)	E(B-V) _{IS} (Luna et al.)	E(B-V) _{IS} (this work)	E(B-V) _{CS} (Luna et al.)
05113+1347	1.1±0.2	0.14	0.310	0.96
05341+0852	1.65±0.09	0.16	0.215	1.49
07134+1005/ 56126	0.4±0.1	0.024	0.080	0.38
17436+5003/ 161796	0.24±0.09	0.026	0.030	0.18
19114+0002/ 179821	0.60±0.05	0.54	0.739	...
19386+0155	1.05±0.09	0.35	0.299	0.80
22223+4327	0.2±0.1	0.21	0.147	...

nential disk with a scale-height of 125 pc (Bonifacio et al. 2000b; Beers et al. 2002), so

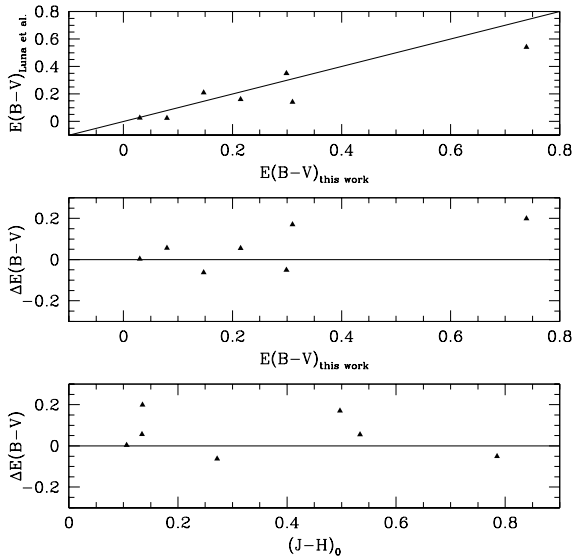


Fig. 3. Representation of the correlation between the colour excess estimated from the maps by Drimmel et al. (2003) and Schlegel et al. (1998) for 7 common objects in both samples (upper panel). The straight line represent a slope to 45 degree. The middle and bottom panel show of E(B-V) residuals as a function of E(B-V) derived by Schlegel et al.’s map and the intrinsic colour (J-H)₀.

$$E(B - V) = [1 - \exp(-|d \sin(b)|/h)] E(B - V)_{NED}, \quad (1)$$

where E(B-V) is the full colour excess for the corresponding star at the distance *d*, *b* is the galactic latitude and *h* is the scale-height of the thin dust disk which adopted 125 pc. For those objects with high and intermediate galactic latitude (*b* > ±10°) we adopt the values calculated by the NED due to the interstellar dust in the line of sight is reduced significantly. A distribution of the total colour excesses found for our sample stars is shown in Figure 2. In this Figure we observe that the total reddening is small for most of the stars studied. This suggests that mostly the redness of the sample come mainly from interstellar component.

In order to check the quality of our E(B-V) estimated from the map of Schlegel et al. (1998), we compare it with the E(B-V) calculated by Luna et al. (2008), which used the Galactic 3D-extinction model map by Drimmel et al. (2003). Both E(B-V) values, named above, reflect only the interstellar component in the light of sight. Table 2 shows the number of stars, the total colour excess observed (taken from Col. 2 of the Table 2 from Luna et al.), the maximum colour excess of the interstellar component derived from Drimmel et al.’s map (taken from Col. 7 of the Table 4 from Luna et al.), the colour excess of the interstellar component obtained from Schlegel et al.’s map (taken from Col. 5 of the Table 2), and the

TABLE 3

JHK_S PHOTOMETRY, THE COLOUR EXCESS AND INTRINSIC COLOURS OF THE
TOTAL STUDY SAMPLE.

Star	J (mag)	H (mag)	K _s (mag)	E(B-V) _{IS}	(J-H) ₀ (mag)	(H-K _s) ₀ (mag)
HD 27381	5.019±0.037	4.747±0.033	4.555±0.016	0.797	0.015	0.046
HD 46703	7.805±0.020	7.513±0.017	7.435±0.018	0.085	0.265	0.062
HD 56126	6.868±0.021	6.708±0.036	6.606±0.017	0.080	0.134	0.087
HD 95767	7.098±0.023	6.532±0.040	5.636±0.023	0.685	0.345	0.771
HD 101584	5.947±0.020	5.138±0.026	3.991±0.260	0.150	0.760	1.119
HD 107369	8.977±0.023	8.844±0.021	8.794±0.021	0.079	0.108	0.036
HD 108015	6.94±0.03	6.38±0.04	5.338±0.027	0.109	0.525	1.022
HD 112374	5.251±0.019	4.856±0.076	4.715±0.017	0.079	0.370	0.127
HD 114855	6.514±0.026	6.173±0.044	6.007±0.021	0.116	0.303	0.144
HD 116745	9.698±0.022	9.481±0.024	9.388±0.020	0.120	0.178	0.071
HD 133656	6.680±0.018	6.524±0.027	6.408±0.020	0.230	0.082	0.074
HD 148743	5.511±0.019	5.358±0.024	5.226±0.023	0.213	0.084	0.093
HD 161796	6.095±0.019	5.979±0.033	5.919±0.017	0.030	0.106	0.055
HD 163506	4.998±0.242	4.239±0.036	3.632±0.280	0.058	0.740	0.596
HD 172481	6.580±0.023	5.877±0.034	5.449±0.017	0.166	0.650	0.398
HD 179821	5.371±0.023	4.998±0.023	4.728±0.020	0.739	0.135	0.135
HD 190390	5.011±0.037	4.639±0.224	4.563±0.017	0.113	0.334	0.048
CpD-625428	9.058±0.020	8.871±0.025	8.774±0.021	0.134	0.144	0.072
IRAS05113+1347	9.020±0.026	8.423±0.018	8.171±0.023	0.310	0.497	0.044
IRAS05341+0852	10.009±0.023	9.405±0.022	9.108±0.021	0.215	0.534	0.045
IRAS07430+1115	8.836±0.021	8.21±0.03	7.766±0.024	0.043	0.612	0.436
IRAS18095+2704	7.366±0.026	6.728±0.017	6.438±0.021	0.099	0.606	0.272
IRAS19386+0155	7.951±0.029	7.069±0.033	6.011±0.023	0.299	0.785	0.062
IRAS22223+4327	7.812±0.018	7.493±0.024	7.246±0.016	0.147	0.272	0.220
HD 82084	5.875±0.019	5.151±0.015	4.367±0.256	0.185	0.664	0.750
HD 105578	7.616±0.026	7.186±0.042	6.917±0.020	0.098	0.397	0.251
HD 107439	7.875±0.019	7.443±0.038	6.759±0.016	0.122	0.393	0.662
HD 170756	5.700±0.018	5.338±0.017	5.075±0.016	0.128	0.319	0.239
AR Pup	7.891±0.029	6.82±0.04	5.285±0.020	0.974	0.757	1.357
AR Sgr	8.412±0.029	7.948±0.044	7.677±0.029	0.153	0.415	0.234
HP Lyr	8.877±0.020	8.429±0.020	7.750±0.024	0.107	0.414	0.659
RX Cap	9.818±0.021	9.463±0.025	9.377±0.021	0.103	0.322	0.067
TX Oph	8.266±0.029	7.846±0.059	7.640±0.018	0.121	0.381	0.184
UY CMa	9.042±0.027	8.597±0.057	7.986±0.026	0.163	0.393	0.581
UZ Oph	8.43±0.05	7.94±0.05	7.791±0.023	0.114	0.453	0.128

minimum colour excess of the circumstellar component (taken from Col. 8 of the Table 4 from Luna et al.). There are only seven common objects in both samples.

Figure 3 shows the correlation between the colour excess derived from both maps (upper panel) and the E(B–V) residuals as a function of colour excess derived from Schlegel et al.’s map, and the intrinsic colour (middle and bottom panel). In the upper panel we see that there are not systematic differences between the two samples and their residuals do not show dependence neither the colour excess nor the intrinsic colour. Our measurements the colour excess are obtained with a mean error of about ± 0.10 .

To determine which of the two components (interstellar or circumstellar) dominates the observed extinction we follow criteria used by Luna et al. (2008). According to Luna et al. (2008) in order to disentangling interstellar and circumstellar extinction in a given source is necessary a statistical approach since it is very difficult to rely only on the available observations. For this we represent E(B–V)_{NED} vs. the galactic distribution of our post-AGB stars and compared them with the sample taken from catalogue of Guarinos (Guarinos 1988a,b; 1997). For further details of this procedure see section 4.3 and Figure 5 in Luna et al. (2008). Only a very small group of objects in the sample present a slight contribution of the circumstellar component. This small group (HD 107369, HD 112374 and 161796) is located at galactic latitude $b > +29$ degrees. At this latitude, the interstellar dust is scarce and the colour excess for these objects are 0.079, 0.079 and 0.030, respectively. This suggests that the contribution circumstellar of these objects is very low.

However, it is very likely that some objects that have a moderate (although possibly significant) contribution from the circumstellar shell to the observed extinction may have escaped to detection or vice-versa (Luna et al. 2008). For example, the case of AR Pup star in which has been detected a large contribution of circumstellar material or BD+39°4926 where was no IR excess detected by IRAS (de Ruyter et al. 2006 and internal references).

In Table 3 we represent the E(B–V) due only to the contribution of interstellar dust along the line of sight. With these values of E(B–V) we can deredden the infrared photometry using the equations of Fiorucci & Munari (2003) for 2MASS photometry. These equations are the following:

$$J_0 = J - 0.887 E(B - V),$$

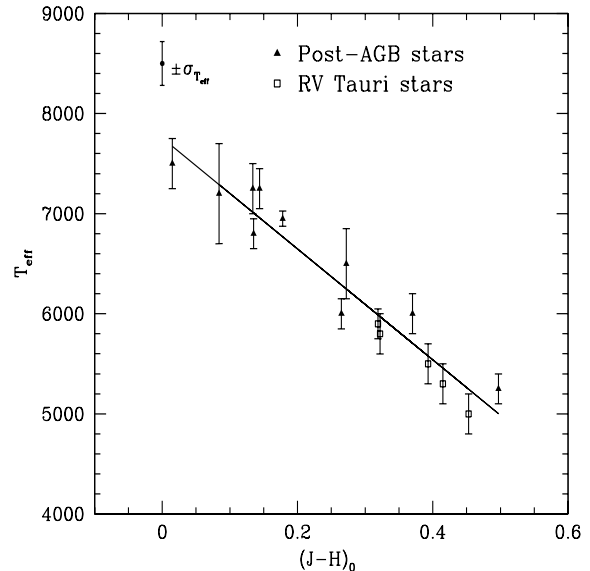


Fig. 4. Representation of the effective temperature against the intrinsic colour. The straight line represent the best fit to the data. The filled triangles represent the post-AGB stars and open squares to the RV Tau stars. The error bars come from the uncertainties in the sample and the T_{eff} relationship.

$$\begin{aligned} (J - H)_0 &= (J - H) - 0.322 E(B - V), \\ (H - K_s)_0 &= (H - K_s) - 0.183 E(B - V). \end{aligned} \quad (2)$$

Table 3 shows the apparent magnitudes and the intrinsic colours for each of our calibrator stars. The mean errors of the observed colours are about 0.114 mag and 0.159 mag in both colours respectively. These were obtained from the correlation between the errors of the observed colours against the intrinsic colours in the near-infrared passband (see Bilir et al. 2008a; Yaz et al. 2010).

4. ATMOSPHERIC PARAMETERS

In this section, we present a set of functional relationships that allow us to derive the atmospheric parameters using the intrinsic colours as independent variables at the infrared region. We use the infrared region because of the infrared colours are less subject to the effect to interstellar absorption.

When the number of independent variables is greater than one we use the method adopted by Stock & Stock (1999). This method developed a quantitative method to obtain stellar physical parameters such as absolute magnitude, intrinsic colour, and a metallicity index using the pseudo-equivalent widths of absorption features in stellar

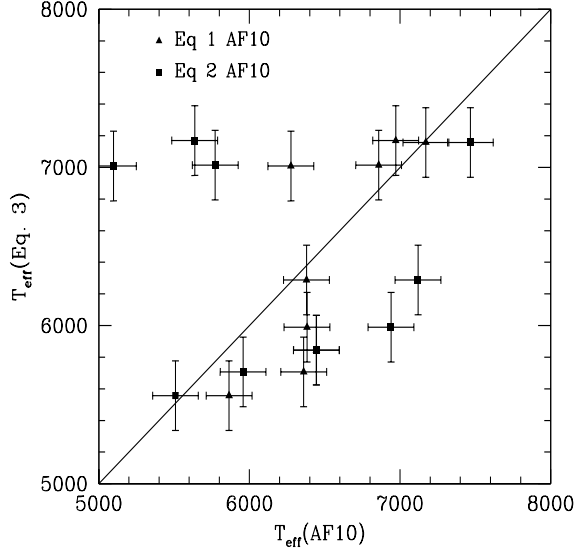


Fig. 5. Representation of the calculated effective temperature estimated by the Eq. (3) against the effective temperature of Equations (1) and (2) from Arellano Ferro (2010). The straight line represent a slope to 45 degree. The error bars come from the uncertainties in the sample and the T_{eff} relationships.

spectra by means of polynomials and a consistent algorithm (Molina & Stock 2004).

4.1. Effective temperature

In order to obtain the effective temperature we use a functional relationship involving only the intrinsic colour $(J-H)_0$. This relationship has the form

$$T_{\text{eff}} = (7756 \pm 126) - (5539 \pm 419)(J-H)_0(3)$$

where this new relationship is valid for a range in effective temperature between $5000 \leq T_{\text{eff}} < 8000$ K and intrinsic colour between $0.00 \leq (J-H)_0 \leq 0.50$, respectively. The correlation between effective temperature and intrinsic colour can be seen in Figure 4. This dependence has been observed by Straizys & Lazauskaite (2009) for a large sample of dwarf and giant stars. The standard deviation derived from the Eq. (3) is ± 220 K.

To verify the values of the effective temperature with an independent method, we compare our values with the calculated effective temperature of the functional relationships (1) and (2) from the work of Arellano Ferro (2010). Figure 5 shows the relationship between the effective temperature obtained by

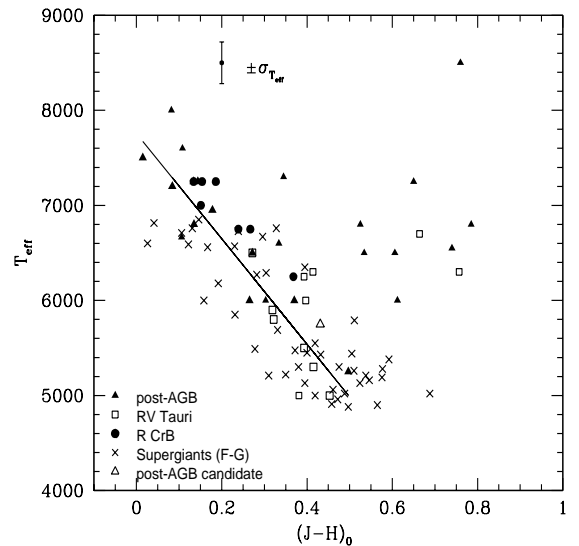


Fig. 6. Representation of some young and evolved sources relative to the T_{eff} vs. $(J-H)_0$ plane. The crosses correspond to variable, double and no-variable young supergiant stars. Filled circles represent R CrB stars. The empty triangle correspond a one post-AGB candidate star. Filled triangles and empty squares represent the post-AGB and RV Tauri of the sample studied. The Eq. (3) which is represented as a solid line. The error bar correspond to a typical uncertainty of ± 220 K in T_{eff} .

the Eq. (3) of this work with respect to the effective temperature derived from Equations (1) and (2) of Arellano Ferro (2010). The error bars show the uncertainties of the functional relationships of both studies. We notice that most of the stars seem to fit with a great dispersion to the slope to 45 degrees.

In Figure 5 we observe that for temperature below 6500 K, the effective temperature calculated from the relationships of Arellano Ferro (2010) appear to be relatively higher than that calculated from Eq. (3). On the contrary for temperature ~ 7000 K the values are more consistent except for three stars HD 46703, HD 56126 and HD 179821 which the Eq. (2) of Arellano Ferro (2010) generates outliers. The temperature values derived from the index $[c_1]$ (filled triangles) seem to fit better to values of temperature calculated from Eq. (3).

In Figure 6 we represent the Eq. (3) and therefore, we analyze the behavior of some young and evolved objects within of the effective temperature versus intrinsic colour plane. The total sample includes young supergiant stars (crosses) obtained from the sample of Arellano Ferro (2010) which have a one post-AGB candidate (empty triangle) star. A set of 7 R CrB stars (filled circles) taken from Stasińska et al. (2006) and the total sample studied of post-AGB (filled triangles) and RV Tauri (empty squares) stars are also included. We observe within the studied range of colours that young supergiant stars show a similar trend but with a large dispersion relative to post-AGB and RV Tauri stars. R CrB stars continue the tendency within the uncertainty of Eq. (3) just like the post-AGB candidate star by their nature post-AGB. However, a large group of objects has a large dispersion and shows no-correlation with Eq. (3).

A possible explanation for the scattering of these objects may come from the poor quality of observed colours, to large errors in the estimated colour excess, or due to a significant contribution of the circumstellar component not detected on these objects: HD 95767, HD 101584, HD 108015, HD 163506, HD 172481 IRAS 05341+0852, IRAS 07430+1115, IRAS 19386+0155, IRAS 18095+2704, HD 82084 and AR Pup. Luna et al. (2008) have pointed out that the reddening of the post-AGB stars of high galactic latitude comes mainly from circumstellar shell not detected in the line of sight. In fact, De Ruyter et al. (2006) has found Keplerian discs of circumstellar dust around post-AGB and RV Tauri stars as HD 95767, HD 108015, HD 163506, HD 82084 and AR Pup. This confirms the hypothesis that most of the redness of these objects come from circumstellar

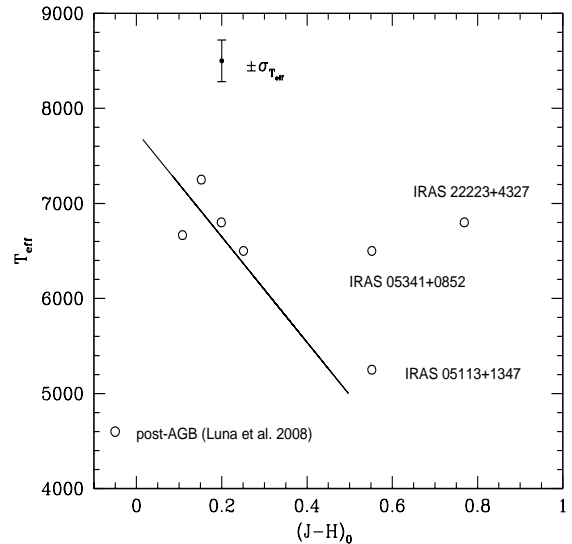


Fig. 7. Representation of seven common objects in the T_{eff} vs. $(J-H)_0$ plane. The empty circles correspond to the sample in Luna et al. (2008). The Eq. (3) is represented as a solid line. The error bar correspond to a typical uncertainty of ± 220 K in T_{eff} .

material.

For the purpose of improving the calibration of the effective temperature from Eq. (3), taking into account what was said above, we suggest two criteria that allow us to restrict those objects evolved primarily dominated from the circumstellar component. First, we should consider the range of validity of Eq. (3), i.e., $5000 \leq T_{\text{eff}} < 8000$ K and $0.00 \leq (J-H)_0 \leq 0.50$, respectively. Second, we should measure the colour excess exclusively dominated by the interstellar component. The mean error in the colour excess of ± 0.10 leads to an uncertainty of about 160 K, this indicates that the greater weight on the uncertainty of the effective temperature come from the colour excess.

Qualitatively this procedure can be seen in Figure 7. This Figure shows the seven common objects which are recorded in Table 2. The Eq. (3) which is represented as a solid line, the error bar corresponds to a typical uncertainty of ± 220 K in T_{eff} , and the empty circles correspond to objects evolved taken from Luna et al. (2008). The intrinsic colour is dominated by the interstellar component derived from Drimmel et al.'s map. We notice that objects with little or nothing of colour excess can be fit to Eq. (3). On the contrary, the objects exclusively dominated by the circumstellar component

(IRAS 05113+1347, IRAS 05341+0852 and IRAS 22223+4327) are clearly away from the calibration. This confirms the validity of Eq. (3) for evolved objects dominated by interstellar components.

4.2. Surface gravity

In order to calculate the gravity we find a linear correlation of the gravity as a function of intrinsic colours $(J-H)_0$ and $(H-K_s)_0$. This has the following form:

$$\begin{aligned} \log g &= (0.78 \pm 0.09) - (0.55 \pm 0.31)(J - H)_0 \\ &+ (0.90 \pm 0.19)(H - K_s)_0. \end{aligned} \quad (4)$$

This relationship is valid for a range of colours between $0.024 \leq (J-H)_0 \leq 1.249$ and $0.062 \leq (H-K_s)_0 \leq 1.431$, respectively. The standard deviation of this relationship is ± 0.27 .

The gravities derived from Eq. (4) in this work are compared with the gravities obtained by Arellano Ferro (2010). In Figure 8 we plot the calculated gravity by the Eq. (4) as a function of the gravity obtained by the Eq. (5) from Arellano Ferro (2010).

In Figure 8 we see that some of the gravities calculated from Eq. (5) generate lowest and highest values of gravity for the range studied (0.0 - 2.0). This may be a consequence that the functional relationship derived from the plane $\log g - \Delta[c_1]$, is valid only for a few RV Tauri (~ 5 stars). It is not the case for post-AGB stars of the sample which follows a different trend than those of young supergiants and RV Tauri stars (Arellano Ferro 2010).

5. ABSOLUTE MAGNITUDE

One of the problems affecting the absolute magnitude in the post-AGB stars is the lack of precise measures of their parallaxes, (e.g., negative parallaxes or very large errors in their parallaxes). Our sample calibrator post-AGB stars and RV Tau stars went through this situation, and even more, in the case of RV Tauri stars no parallax determination existed for some of them.

The interstellar extinction for the stars in the direction of the galactic plane is another problem when we estimate the absolute magnitude. We use the corrected parallaxes of van Leeuwen (2007) to calculate the absolute magnitudes for a group of stars (Table 4). The absolute magnitude of the stars in the Table 4 have been computed by the well-known distance-modulus formula in the near-infrared M_J band:

$$M_J = J_0 - 5 \log(1/\pi) + 5. \quad (5)$$

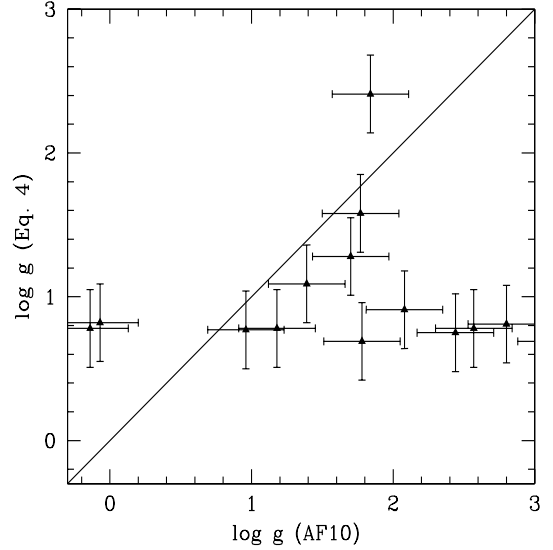


Fig. 8. Representation of the calculated surface gravity by the Eq. (4) as a function of surface gravity derived by the Eq. (5) from Arellano Ferro (2010). The comment that follows is similar to Figure 5.

In the estimation of the absolute magnitude we propose a functional relationship where M_J is a function of intrinsic colours of the following form:

$$\begin{aligned} M_J &= -(6.00 \pm 0.35) + (11.47 \pm 4.30)(J - H)_0 \\ &- (17.00 \pm 3.13)(J - H)_0^2 + (3.07 \pm 0.39) \\ &(H - K_s)_0. \end{aligned} \quad (6)$$

The standard deviation of the absolute magnitude in the near-infrared band is about 0.28 mag. This value would lead to a parallax error (σ_π/π) of about 20% or less. The Eq. (6) is valid for a range of colours between $0.015 \leq (J-H)_0 \leq 0.761$ and $0.046 \leq (H-K_s)_0 \leq 1.357$, respectively. The near-infrared region promises a better estimation of the absolute magnitude for post-AGB and RV Tauri stars. In fact, Bilir et al. (2008b) has observed the sensitivity of the intrinsic colours in the near-infrared band to the absolute magnitude to a group of 44 detached binaries. Table 4 shows the parallax π , the parallax error $\Delta\pi$, the distance d , the interstellar extinction $E(B-V)$ and the absolute magnitude M_J in the near-infrared band. We can observe that the large errors on the parallaxes and the colour excesses leads to a large error for the distance and absolute magnitude determinations, i.e. HD 179821.

Figure 9 shows the estimated absolute magnitude of the Eq. (6) against the absolute magnitude calcu-

TABLE 4
 FUNDAMENTAL DATA USED IN THE DETERMINATION OF THE ABSOLUTE
 MAGNITUDE IN THE NEAR-INFRARED BAND.

Star	π (mas)	$\Delta\pi$ (mas)	d (pc)	E(B-V)	M_J (mag)
HD 27381	1.03	0.98	971	0.797	-5.62
HD 46703	0.89	1.02	1124	0.085	-2.52
HD 101584	1.35	0.64	741	0.150	-3.53
HD 105578	0.61	1.13	1639	0.098	-3.54
HD 114855	2.32	1.06	431	0.116	-1.76
HD 148743	0.73	0.43	1370	0.213	-5.36
HD 163506	0.76	0.23	1316	0.058	-5.65
HD 170756	0.53	1.40	1887	0.128	-5.79
HD 179821	0.18	1.12	5556	0.739	-9.01
HD 190390	1.38	0.42	725	0.113	-4.39
AR Pup	2.21	1.23	452	0.974	-1.25

lated by two different methods from de Ruyter et al. (2006).

De Ruyter et al. (2006) carried out a homogeneous and systematic study of the Spectral Energy Distributions (SEDs) of a sample of post-AGB and RV Tauri objects, assuming the circumstellar dust is stored in Keplerian rotating passive discs. Some of these objects are considered post-AGB binary stars and also include new RV Tauri star candidates. In determining the distance the authors used the relationship P-L from Alcock et al. (1998) derived for a set of RV Tauri stars in the Large Magellanic Cloud (LMC) with a defined period of pulsation. For those objects that do not have a defined period of pulsation, Ruyter et al. (2006) took a constant relationship in determining the luminosity,⁵ assuming that the typical luminosity of a lower mass post-AGB star is expected to be between 1000 and 10 000L_⊙. Consequently, the uncertainties for the luminosity and the distances obtained by both methods are significant. The results of these distances and uncertainties are shown in their Ruyter et al., Table A.2.

On the other hand, to verify the level of reliability of Eq. (6) we apply our method to the sample of post-AGB and RV Tauri studied by the de Ruyter et al. (2006). This procedure takes place because our sample has very few common objects in relation to the sample from de Ruyter et al. (2006). We studied about 36 stars of a total sample of 51 post-AGB and RV Tauri stars contained within the A-G spectral range. We identify the JHK_s colours ob-

served from the 2MASS source and it was found the intrinsic colours (J-H)₀ and (H-K)₀ from the excess color derived for the sample (see Ruyter et al., Table A.1). Finally, the absolute magnitudes are derived from Equations (5) and (6).

In Figure 9 we observe that a majority of the sample objects with a known period P (open squares), the absolute magnitude M_J derived of the distance has a tendency to adjust to the results obtained from our functional relationship within $M_J \leq -2$ mag. This indicates that the Eq. (6) can be applied to binary or variables objects. However, most of the objects without pulsation period (filled triangle) and whose distances were derived assuming a typical luminosity of a post-AGB star of low-mass, the absolute magnitudes tend to be larger than the absolute magnitudes derived from the Eq. (6) and are clustered in the range between $0 \leq M_J \leq -4$ mag. The systematic differences observed for the latter group may be probably due to differences in the masses of these objects.

6. DISCUSSION AND CONCLUSION

The study of a sample of post-AGB and RV Tauri stars has led to find out a set of empirical relationships that allow us to estimate the physical parameters as the effective temperature and the gravity with precision of 220 K and 0.27, respectively. Effects of variability and pulsation in RV Tauri and post-AGB stars affect very little to temperature and gravity calibrations. In fact, few of them are out of calibrations, e.g., in Teff, HD 82084, AR Pup, HD 108015, HD 163506, and HD 172481. These

⁵L = (5000 ± 2000)L_⊙

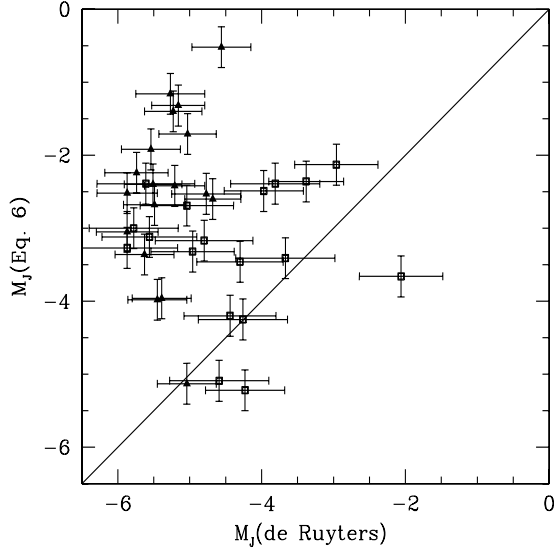


Fig. 9. Absolute magnitudes predicted by the equation (6) versus near-infrared absolute magnitudes obtained of distances from de Ruyter et al. (2006). The empty squares represent the absolute magnitudes for stars that have a defined period P while filled triangles represent those stars without determined pulsation period P .

uncertainties derived from our effective temperature and gravity calibrations are comparable with those derived by Arellano Ferro (2010) who used $ubvvy\beta$ -photometry. These equations cover a wide range of colours in the near-infrared band and it can be valid for variables, no-variables and/or semi-regular pulsating objects with low-interstellar extinction and low-masses. Furthermore, these functional relationships can be extended to R CrB stars with a rare H-deficient. In addition, for young supergiant stars it can not be deduced their atmospheric parameters with high precision.

For those very reddening objects whose central star is visible in the optical it is possible to obtain a better estimation of their temperature and gravity if we study the diffuse bands of the circumstellar material around these stars in order to correct the effects of circumstellar reddening according to the procedure by Luna et al. (2008).

In Figure 2, we also observe that the colour excess of most stars due to interstellar dust is small, so that the reddening present in some post-AGB and RV Tauri objects such as HD 95767, HD 101584, HD 108015, HD 163506, HD 172481, IRAS 05341+0852, IRAS 07430+1115, IRAS 19386+0155,

IRAS 18095+2704, HD 82084 and AR Pup comes likely from circumstellar dust not detected stored in Keplerian discs around them (de Ruyter et al. 2006). On the contrary, The effect of circumstellar reddening observed in the post-AGB stars such as HD 107369, HD 112374 and HD 161769 appears to be minimal since it does not affect the de-reddened colours.

On the other hand, the absolute magnitude in the near-infrared J-band promises to be recovered satisfactorily. In fact, the magnitude absolutes of RV Tauri stars obtained from the P–L relation are consistent within a large dispersion to the absolute magnitudes estimated in this work. This indicates that the P–L relation could be also applicable to field stars. The Hipparcos parallax could be the main cause contributing to the generation of the dispersion in Eq. (6), but there are also other uncertainties that are present as the errors in the excess of colour and the intrinsic colour. Similarly, the propagation of errors from the P–L relation leads to uncertainties in the luminosities and hence, in distances. Finally, the dust surrounding the star seen nearly edge-on also affects the luminosity when using the P–L relation.

We notice that for stars without defined pulsation period, the approach all the stars may have the same luminosity is not valid because, as shown in Figure 9 absolute magnitudes derived from the Eq. (6) vary between a range from $0 \leq M_J \leq -4$ mag. This indicates that this group of stars do not have neither the same stellar masses nor an unique value of luminosity ($L = 5000L_{\odot}$).

In short, an alternative way to achieve real improvements in the estimation of the absolute magnitude could be the use of high resolution spectroscopic techniques (see Arellano Ferro 2003) or expected precise measurements of parallaxes in the future through the GAIA mission.

Acknowledgments

This work has made extensive use of SIMBAD database and the ADS-NASA to which we are thankful. I would also like to thank to Dr. Anibal García Hernández and Dr. Jesús Hernández for very useful and fruitful comments and suggestions on the manuscript. The author thank to an anonymous referee for helpful suggestions. I would also like to thank Prof. Luz Angela Cañas for her valuable English corrections.

REFERENCES

Alcock, C., Allsman, R.A., Alves, D.R. et al. 1998, AJ, 115, 1921

- Arce, H.G. & Goodman, A.A., 1999, *ApJ*, 512, L135
- Arellano Ferro, A. & Parrao, L., 1990, in *Confrontation between Stellar Pulsation and Evolution*, ASP Conf. Ser. 11, 218
- Arellano Ferro, A. & Mantegazza, L., 1996, *A&A*, 315, 542
- Arellano Ferro, A., Giridhar, S., Mathias, P., 2001, *A&A*, 368, 250
- Arellano Ferro, A., Giridhar, S., Rojo Arellano E., 2003, *RMA&A*, 39,3
- Arellano Ferro, A., 2010, *RMA&A*, 46, 331
- Beers, T.C., Drilling, J.S., Rosi, S., et al., 2002, *AJ*, 124, 931
- Bessell, M.S. & Brett, J.M., 1988, *PASP*, 100, 113
- Bilir, S., Ak, S., Karaali, S., Cabrera-Lavers, A., Chonis, T.S., Gaskell, C.M., 2008a, *MNRAS*, 384, 1178
- Bilir, S., Ak, T., Soydogan, F., Yaz, E., Filiz, A.N., Eker, Z., Demircan, O., Helvacı, M., 2008b, *Astron Nachr*, 329, 835
- Bilir, S., Karaali, S., Ak, S., Coskunoglu, K.B., Yaz, E., Cabrera-Lavers, A., 2009, *MNRAS*, 396, 1589
- Bonifacio, P., Caffau, E., Molaro, P., 2000b, *A&AS*, 145, 473
- Bonifacio, P., Monai, S. & Beers, T.C., 2000a, *AJ*, 120, 2065
- Bravo-Alfaro, H., Arellano Ferro, A., Schuster, W. H., 1997, *PASP*, 109, 958
- Cenarro, A.J., Peletier, R.F., Sánchez-Blázquez, P., Selam, S.O., Toloba, E., Cardiel, N., 2007, *MNRAS*, 374, 664
- Covey, K.R., Ivezić, Ž., Schlegel, D., Finkbeiner, D., Padmanabhan, N., et al., 2007, *AJ*, 134, 2398
- Cutri, R.M., et al., 2003, *VizieR On-Line Data Catalog: II/246*
- Decin, L., Van Winckel, H., Waelkens, C., Bakker, E.J., 1998, *A&A*, 332, 928
- Drimmel R., Cabrera-Lavers A. & López-Corredoira M. 2003, *A&A*, 409, 205
- Fiorucci, M, Munari, U., 2003, *A&A*, 401, 781
- Giridhar, S., Lambert, D.L., González, G., 1998, *ApJ*, 509, 366
- Giridhar, S., Rao, N.K., Lambert, D.L., 1994, *ApJ*, 437, 476
- Giridhar, Sunetra, Arellano Ferro, A., 2005, *A&A*, 443, 297
- Giridhar, S., Lambert, D. L., Reddy, B. E., Gonzalez, G., Yong, D., 2005, *ApJ*, 627, 432
- Giridhar, S., Molina, R., Arellano Ferro, A., Selmakumar, G., 2010, *MNRAS*, 406, 290
- González, G., Wallerstein, G., 1992, *MNRAS*, 254, 343
- González, G., Lambert, D.L., Giridhar, S., 1997a, *ApJ*, 479, 427
- Guarinos, J. 1988a, *Bull. d'inf. cent. données stellaires*, 35, 161
- Guarinos, J. 1988b, *Bull. d'inf. cent. données stellaires*, 34, 14
- Guarinos, J. 1997, *VizieR On-line Data Catalog: II/135*
<http://vizier.u-strasbg.fr/viz-bin/VizieR>
- Hrivnak, B.L., Reddy, B.E., 2003, *ApJ*, 590, 1049
- Jura, M., 1986, *ApJ*, 309, 732
- Luck, R.E., Lambert, D.L., Bond, H.E., 1983, *PASP*, 95, 413
- Luck, R.E., Bond, H.E., Lambert, D.L., 1990, *ApJ*, 357, 188
- Luck, R.E. & Bond, H.E., 1984, *ApJ*, 279, 729
- Luna, R., Cox, N.L.J., Satorre, M.A., García Hernández, Suarez, O. & García Lario, P. 2008, *A&A*, 480, 133
- Lyubimkov, L.S., Lambert, D.L., Rostopchin, S.I., Rachkovskaya, T.M., Poklad, D.B., 2010, *MNRAS*, 402, 1369
- Mass, T., van Winckel, H., Waelkens, C., 2002, *A&A*, 386, 504
- Molina, R. & Stock, J., 2004, *RMxA&A*, 40, 181
- Pereira, C.B., Lorentz-Martins, S. & Machado, M., 2004, *A&A*, 422, 637
- Pickles, A.J., 1998, *PASP*, 110, 863
- Preston, G.W., Krzeminski, W., Smak, J., Williams, J.A., 1963, *ApJ*, 137, 401
- Reddy, B., Bakker, E.J., & Hrivnak, B.J., 1999, *AJ*, 117, 1834
- Reddy, B.E., Lambert, D.L., González, G., Yong, D., 2002, *ApJ*, 564, 482
- De Ruyters, S., van Winckel, H., Maas, T., Lloyd Evans, T., Waters, L.B.F.M. and Dejonghe, H., 2006, *A&A*, 448, 641
- Sahin, T., Lambert, D.L., Klochkova, L., Tavolganskaya, N.S., 2011, *MNRAS*, 410, 612
- Schlegel, D.J., Finkbeiner, D.P., Davis, M., 1998, *ApJ*, 500, 525
- Sivarani, T., Parthasarathy, M., García-Lario, P., Manchado, A., Pottash, S.R., 1999, *A&A*, 137, 505
- Stasińska, G., Szczerba, R., Schmidt, M., Siodmiak, N., 2006, *A&A*, 450, 701
- Stock, J. & Stock, J.M., 1999, *RMA&A*, 35, 143
- Straizys, V., Lazauskaite, R., 2009, *Baltic Astronomy*, 18, 19
- Van Leeuwen, F., 2007, *A&A*, 474, 653
- Van Winckel, H., Oudmaijer, R.D., & Trams, N.R., 1996, *A&A*, 312, 553
- Van Winckel, H. & Reyniers, M., 2000, *A&A*, 354, 135
- Van Winckel, H., Decin, L., & Waelkens, C., 1997, *IAUS*, 189P, 176V
- Wahlgren, G.M., 1993, in *Luminous High-Latitude Stars*. P.S. Conference Series, D. Sasselov (ed), 45, p. 270
- Yasuda, N., Fukugita, M. & Schneider, D.P., 2007, *AJ*, 134, 698
- Yaz, E., Bilir, S., Karaali, S., Ak, S., Coskunoglu, K.B., Cabrera-Lavers, A., 2010, *Astron Nachr*, 331, 807
- Zač, L., Klochkova, V.G., Panchuk, V.E., Spelmanis, R., 1996, *MNRAS*, 282, 1171

R. E. Molina: Laboratorio de Investigación en Física Aplicada y Computacional, Universidad Nacional Experimental del Táchira, Venezuela, (rmolina@unet.edu.ve).